Quantitative prediction of excited-state decay rates for radical anion photocatalysts

Leandro D. Mena,[a,b] Jose L. Borioni,[a,b] Sofia Caby,[a,b] Patrick Enders,[c,d] Miguel A. Argüello Cordero,[e] Franziska Fennel,[e] Robert Francke,[c,d] Stefan Lochbrunner,[e] and Javier I. Bardagi*[a,b]

[a]*Instituto de Investigaciones en Fisicoquímica de Córdoba, Córdoba, Argentina (INFIQC-CONICET).*

[b]*Departamento de Química Orgánica, Facultad de Ciencias Químicas, Universidad Nacional de Córdoba, Ciudad Universitaria, X5000HUA, Córdoba, Argentina.*

[c]*Leibniz Institute for Catalysis, Albert-Einstein-Str. 29a, 18059 Rostock, Germany.*

[d]*Institute of Chemistry, Rostock University, 18059 Rostock, Germany.*

[e]*Institute for Physics and Department of Life, Light and Matter, University of Rostock, 18051 Rostock, Germany.*

E-mail: jbardagi@unc.edu.ar

1. General Procedures

1.1. Reagents, materials and general experimental methods

Naphthalene-1,4,5,8-tetracarboxylic acid anhydride (NDA), *N*-hexylamine (99%), *N*-octylamine (99%), aniline, *p*-toluidine hydrochloride, 3-aminopentane, and pyridine were used without further purification. Acetonitrile (ACN) was HPLC grade. All other chemicals and solvents were purchased from commercial suppliers and used as received without further purification.

^{1}H NMR spectra were recorded on a spectrometer at 400 MHz. Chloroform ($CDCl_3$ 99.8 atom% D) was used as solvent. ^{1}H NMR data are reported as follows: chemical shift (ppm), multiplicity (s = singlet, d = doublet, dd = doublet of doublets, t = triplet, m = multiplet), coupling constants (Hz) and integration for known compounds.

2. Structures of radical anion precursors used in this study

2.1. Compounds previously measured

Gosztola, D.; Niemczyk, M. P.; Svec, W.; Lukas, A. S.; Wasielewski, M. R. *J. Phys. Chem. A* **2000**, *104* (28), 6545–551 https://doi.org/10.1021/jp000706f

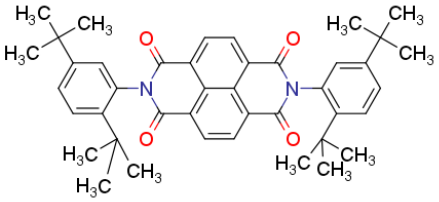

NDI1

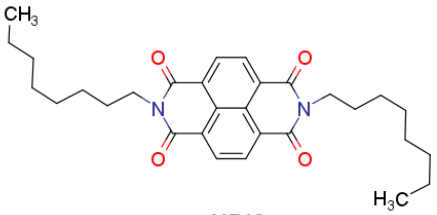

NDI2

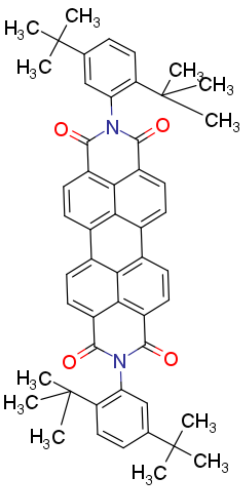

PDI1

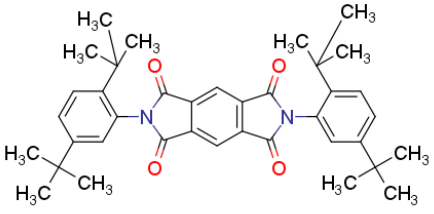

FDI1

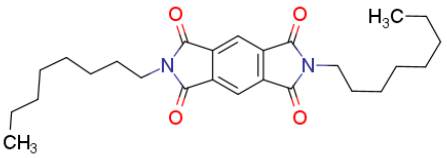

FDI2

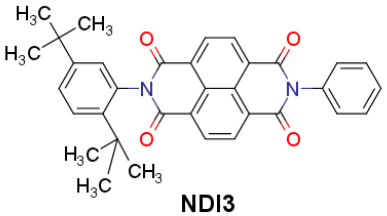

NDI3

N. T. La Porte, J. A. Christensen, M. D. Krzyaniak, B. K. Rugg and M. R. Wasielewski, *J. Phys. Chem. B*, **2019**, 123, 7731–739. https://doi.org/10.1021/acs.jpcb.9b06303.

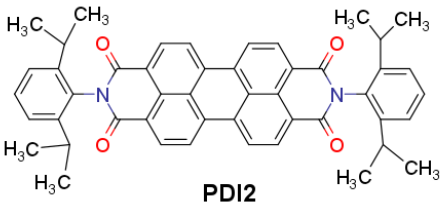

PDI2

C. J. Zeman, S. Kim, F. Zhang and K. S. Schanze, *J. Am. Chem. Soc.*, **2020**, 142, 2204–207. https://doi.org/10.1021/jacs.9b13027

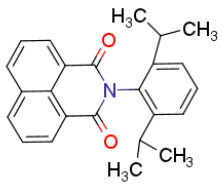

NMI

A. J. Rieth, M. I. Gonzalez, B. Kudisch, M. Nava and D. G. Nocera, *J. Am. Chem. Soc.*, **2021**, 143, 14352–4359. https://doi.org/10.1021/jacs.1c06844

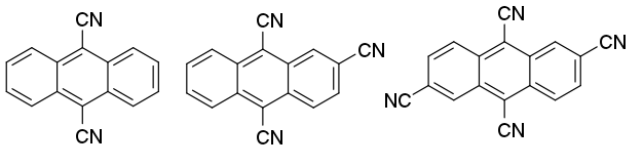

DCA TrCA TCA

Beckwith, J. S.; Aster, A.; Vauthey, E. *Phys. Chem. Chem. Phys.* **2022**, *24* (1), 568–77. https://doi.org/10.1039/D1CP04014F

Figure S1. Structures of phenyl diimides (FDA), naphtalene diimides (NDI), perylene diimides (PDI), naphthalene monoimides (NMI) and polycyanoanthracenes (DCA, TrCA and TCA).

2.2. Compounds measured in this work

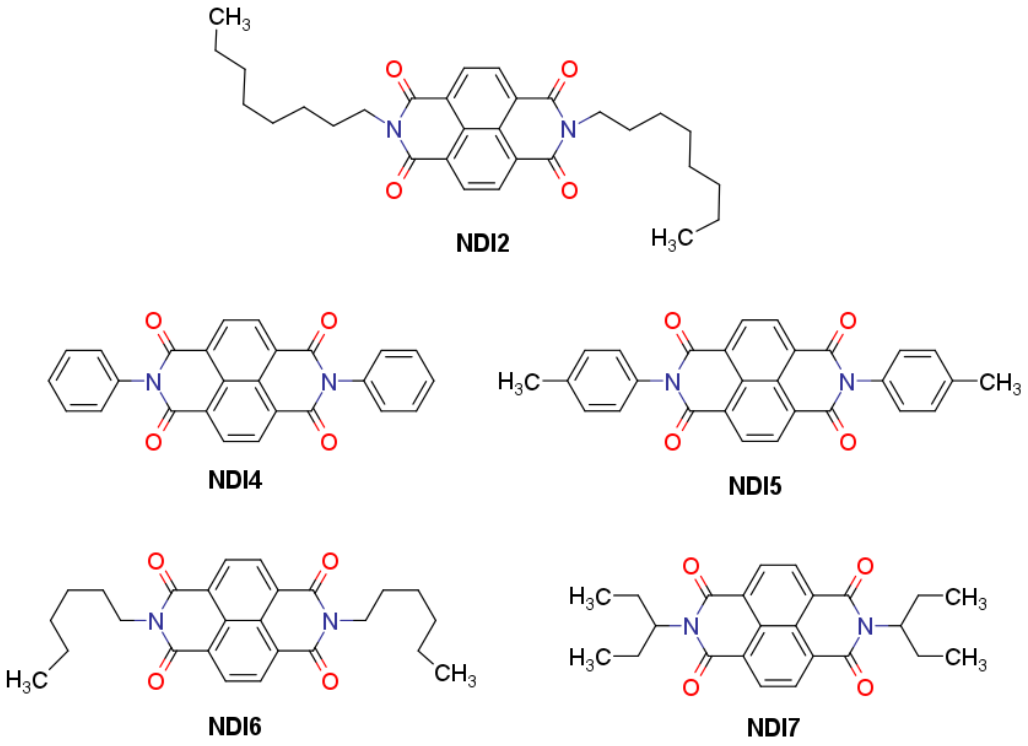

Figure S2. Structures of naphthalene diimides (NDI) synthesized in this work.

3. Synthesis and characterization of naphthalene diimides

3.1. Synthesis of NDI

Synthesis started from commercially available naphthalene-1,4,5,8-tetracarboxylic acid anhydride (NDA) and the corresponding amine using reported procedures (Scheme S1).[37]

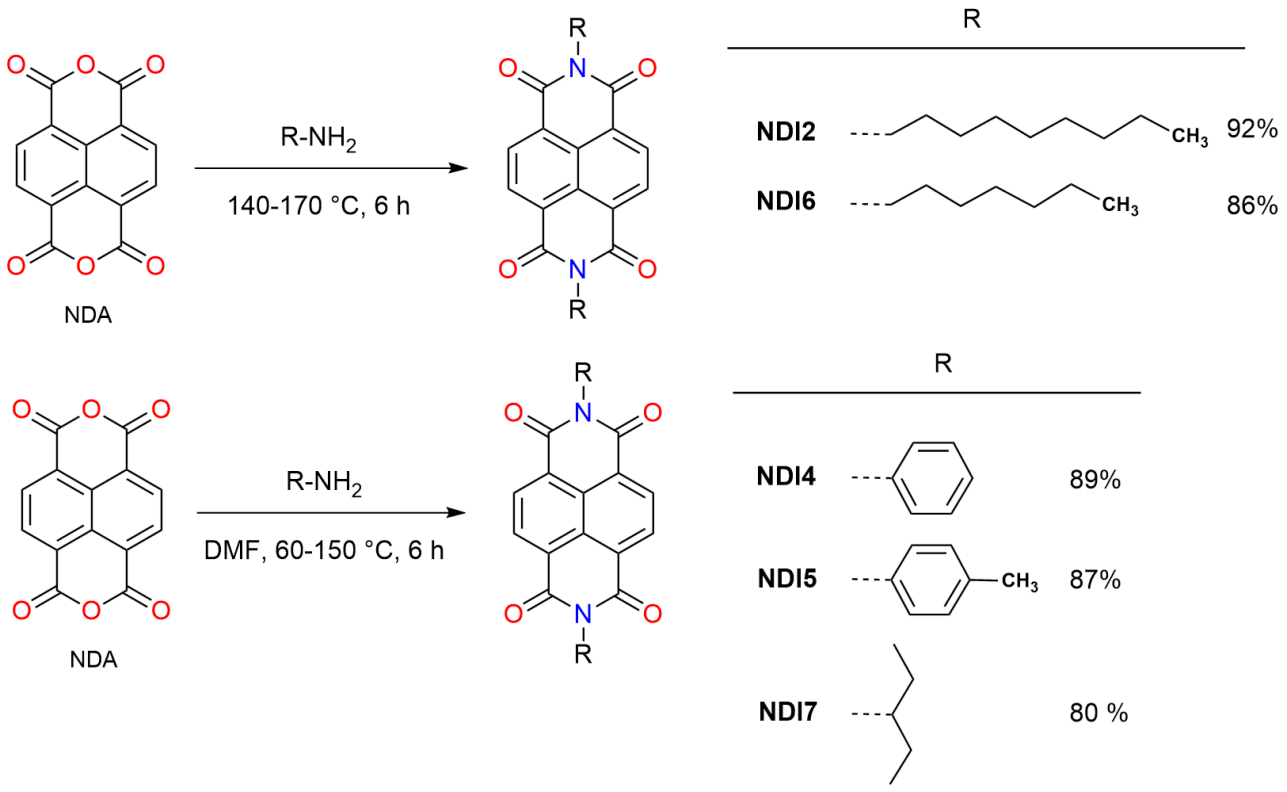

Scheme S1. Synthesis of **NDI1-7**.

2,7-Dioctylbenzo[*lmn*][3,8]phenanthroline-1,3,6,8(2*H*,7*H*)-tetraone (NDI2):

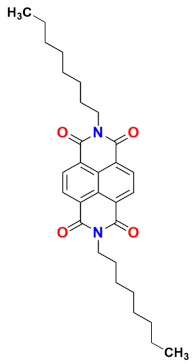

A 10 mL round bottom flask was equipped with a magnetic stir bar and was charged with NDA (2 mmol, 1 equiv.) and *n*-octylamine (7 mL, 43 mmol, 22 equiv.). The resulting mixture was heated to 170 °C for 6 h. After cooling to room temperature, the solid obtained was filtered and washed with hexane affording NDI3 as a pale brown solid (902 mg, 92% yield).

Identity and purity of the product were confirmed by ^{1}H NMR, ^{13}C NMR and GC-MS.

^{1}H NMR (CDCl$_3$, 400 MHz, TMS): δ= 8.78 (s, 4H), 4.21 (m, 4H), 1.76 (m, 4H), 1.49-1.30 (m, 20H), 0.90 (t, *J* = 6.8 Hz, 6H). **^{13}C NMR (CDCl$_3$, 101 MHz):** δ= 162.8, 130.9, 126.7, 41.0, 31.8, 29.3, 29.2, 28.1, 27.1, 22.6, 14.0. **GC-MS (DI) m/z (%):** 491 (33) [*M*+1]$^{+}$, 490 (100) [*M*+], 380 (21), 379 (41), 281 (14), 268 (12), 267 (14), 249 (21), 69 (66), 55 (31). Data is in accordance with the literature.[1]

2,7-diphenylbenzo[*lmn*][3,8]phenanthroline-1,3,6,8(2*H*,7*H*)-tetraone (NDI4)[2]

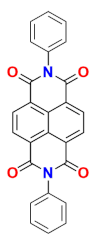

A 250 mL round bottom flask was equipped with a magnetic stir bar and was charged with NDA (15 mmol, 1 equiv.), DMF (100 mL) and aniline (3.7 mL, 40 mmol, 2.7 equiv.). The resulting mixture was heated to 150 °C for 6 h. After cooling to room temperature, the solid obtained was filtered and washed with *n*-heptane affording NDI4 as a pale brown solid (5.6 g, 89% yield).

Identity and purity of the product were confirmed by ^{1}H NMR, ^{13}C NMR and GC-MS.

^{1}H NMR ($CDCl_3$, 300 MHz, TMS): δ= 8.79 (s, 4H), 7.56 – 7.44 (m, 6H), 7,30-7.27 (m, 4H). **^{13}C NMR ($CDCl_3$, 75 MHz):** δ= 163.2, 131.7, 129.6, 129.3, 128.5, 127.1. **GC-MS (DI) m/z (%):** $[M+1]^+$ 419 (29), $[M+]^+$ 418 (100), 417 (80), 325 (15), 77 (11). Data is in accordance with the literature.

2,7-di-*p*-tolylbenzo[*lmn*][3,8]phenanthroline-1,3,6,8(2*H*,7*H*)-tetraone (NDI5)[2]

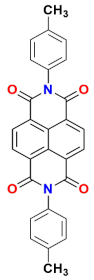

A 250 mL round bottom flask was equipped with a magnetic stir bar and was charged with NDA (15 mmol, 1 equiv.), DMF (100 mL), *p*-toluidine hydrochloride (40 mmol, 2.7 equiv.) and pyridine (40 mmol, 2.7 equiv.). The resulting mixture was heated to 150 °C for 6 h. After cooling to room temperature, the solid obtained was filtered and washed with *n*-heptane affording NDI5 as a pale yellow solid (5.9 g, 87% yield).

Identity and purity of product were confirmed by ^{1}H NMR, ^{13}C NMR and GC-MS.

^{1}H NMR ($CDCl_3$, 300 MHz, TMS): δ= 8.77 (s, 4H), 7.32 (dd, J = 8.5, 0.5 Hz, 4H), 7.18 – 7.12 (m, 4H), 2.40 (s, 6H). **^{13}C NMR ($CDCl_3$, 75 MHz):** δ= 163.2, 139.3, 131.9, 131.4, 130.3, 128.1, 127.1, 21.4. **CG-MS (ID) m/z (%):** $[M+1]^+$ 447 (33), $[M+]^+$ 446 (100), 445 (51), 339 (26).

Data is in accordance with literature.

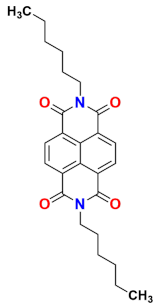

2,7-Dihexylbenzo[*lmn*][3,8]phenanthroline-1,3,6,8(2*H*,7*H*)-tetraone (NDI6):[3]
A 10 mL round bottom flask was equipped with a magnetic stir bar and was charged with NDA (2 mmol, 1 equiv.) and *n*-hexylamine (7 mL, 53 mmol, 27 equiv.). The resulting mixture was heated to 140 °C into an oil bath for 6 h. After cooling to room temperature, the solid obtained was filtered and washed with hexane, affording NDI as a pale pink solid in 86% yield.
Identity and purity of product were confirmed by ^{1}H NMR, ^{13}C NMR and GC-MS.

^{1}H NMR ($CDCl_3$, 400 MHz, TMS): δ= 8.77 (s, 4H), 4.21 (m, 4H), 1.76 (m, 4H), 1.49-1.27 (m, 12H), 0.92 (t, *J* = 7.0 Hz, 6H). **^{13}C NMR ($CDCl_3$, 101 MHz):** δ= 162.8, 130.9, 126.7, 41.0, 31.5, 28.0, 26.7, 22.5, 14.0. **GC-MS (DI) m/z (%):** 435 (29) $[M+1]^+$, 434 (100) $[M+]$, 364 (12), 352 (19), 351 (48), 281 (18), 280 (12), 268 (12), 167 (18), 249 (28), 83 (23), 55 (41). Data is in accordance with the literature.

2,7-Di(pentan-3-yl)benzo[*lmn*][3,8]phenanthroline-1,3,6,8(2*H*,7*H*)-tetraone (NDI7)[4]

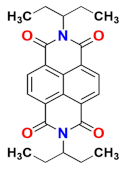

A 25 mL round bottom flask was equipped with a magnetic stir bar and was charged with NDA (15 mmol, 1 equiv.), DMF (10 mL) and 3-aminopentane (5 mL, 43 mmol, 2.8 equiv.). The resulting mixture was heated to 60 °C for 6 h. After cooling to room temperature, the solid obtained was filtered and washed with *n*-heptane affording NDI4 as a pale yellow solid (5.9 g, 80% yield).

Identity and purity of product were confirmed by ^{1}H NMR, ^{13}C NMR and GC-MS.

^{1}H NMR ($CDCl_3$, 400 MHz, TMS): δ= 8.72 (s, 4H), 5.02 (tt, J = 9.6, 5.9 Hz, 2H), 2.34 – 2.09 (m, 4H), 2.05 – 1.78 (m, 4H), 0.89 (t, J = 7.5 Hz, 12H). **^{13}C NMR ($CDCl_3$, 101 MHz):** δ= 163.7, 130.9, 126.8, 58.13, 24.95, 11.2. **CG-MS (ID) m/z (%):** $[M+1]^+$ 407 (16), $[M+]^+$ 406 (55), 377 (20), 338 (25), 337 (100), 307 (14), 267 (27), 249 (27), 55 (10).

Data is in accordance with the literature.

3.2. Electrochemical properties of NDI

Cyclic voltammetry. The experiments were carried out in a custom-made three-electrode cell using a PGSTAT 302N (Autolab, Metrohm). A glassy carbon disk (diameter: 1.6 mm) served as the working electrode and a platinum wire as

the counter electrode. The glassy carbon disk was polished using polishing alumina (0.05 μm) prior to each experiment. As reference, a $Ag/AgNO_3$ electrode (silver wire in 0.1 M n-Bu_4NClO_4/CH_3CN solution; $c(AgNO_3)$ = 0.01 M; E_0 = −87 mV *vs.* ferrocene/ferrocenium couple)[5] was used, and this compartment was separated from the rest of the cell with a Vycor frit. Unless noted otherwise, a solution of n-Bu_4NBF_4 (0.1 M, electrochemical grade) in ACN was used as the electrolyte. The electrolyte solution was purged with Ar for at least 5 min prior to recording. The reduction potentials (E) were extracted from background corrected voltammograms. To account for the iR drop at high scan rates, positive feedback iR compensation was used. The resistance R was determined by electrochemical impedance spectroscopy prior to each experiment.

Table S1. Reduction Potentials of synthesized NDIs

Compound	***E vs.* Ag/AgNO$_3$(0.01 M) (V)**		***E* (NDI/NDI$^{\bullet-}$) *vs.* NHE**
	NDI/NDI$^{\bullet-}$	**NDI$^{\bullet-}$/NDI^{2-}**	
NDI2	-0.92	-1.34	-0.37
NDI4	-0.87	-1.28	-0.32
NDI5	-0.88	-1.29	-0.33
NDI6	-0.92	-1.34	-0.37
NDI7	-0.94	-1.41	-0.39

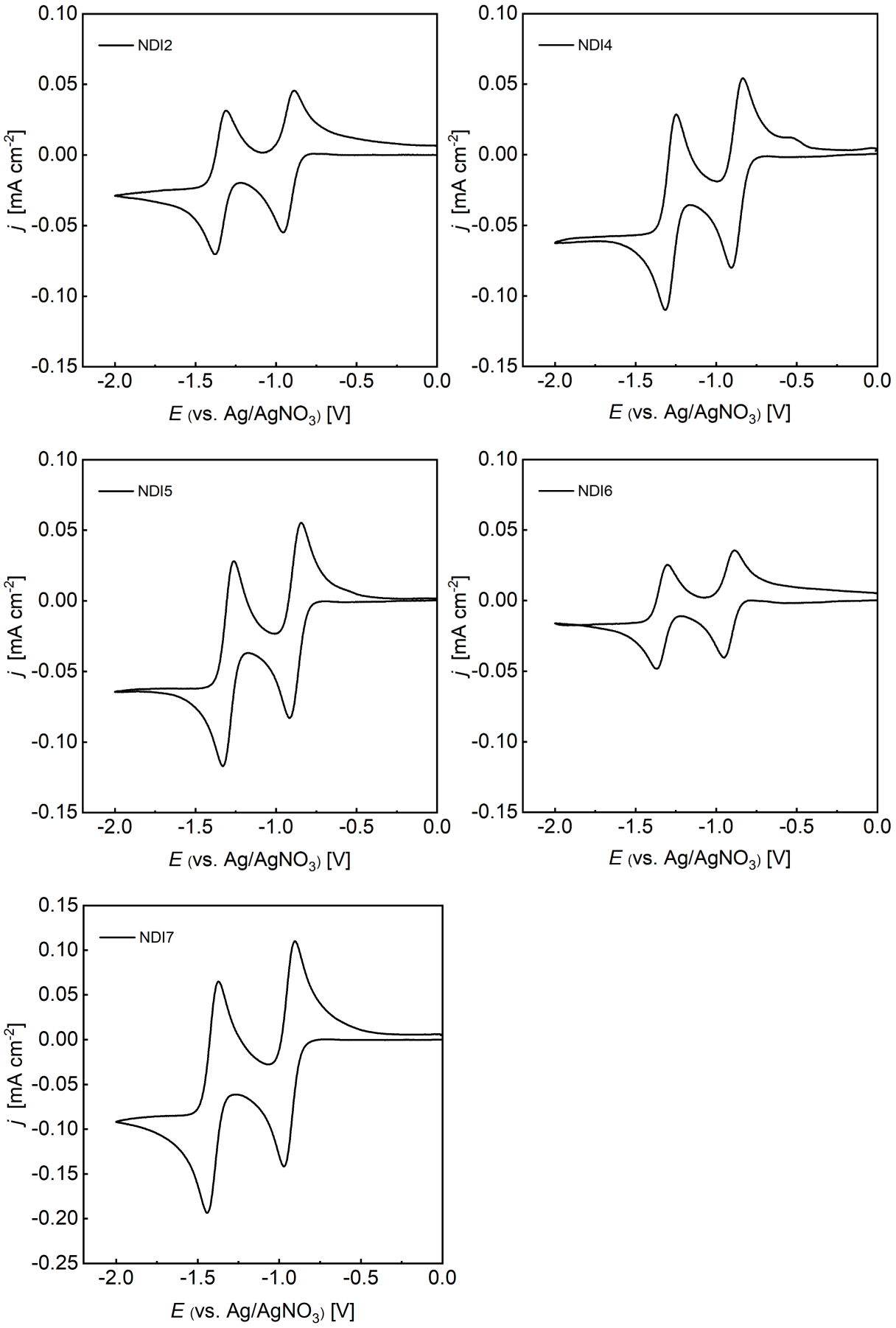

Figure S3. Cyclic voltammetry of naphthalene diimides (NDI) synthesized in this work.

4. Stationary and time resolved spectroscopy of naphthalene diimide radical anions

4.1. Electrochemical preparation of radical anions

The experiments were carried out in a custom made three-electrode H-cell using either a PGSTAT 302N (Metrohm Autolab) or a PGSTAT 128N (Metrohm Autolab). A glassy carbon plate (70 mm x 10 mm x 3 mm) was used as the working electrode and a platinum sheet (70 mm x 10 mm x 3 mm) as the counter electrode. As reference, a $Ag/AgNO_3$ electrode (silver wire in 0.1 M NBu_4BF_4 CH_3CN solution; c($AgNO_3$) = 0.01 M; E_0 = −87 mV *vs.* ferrocene/ferrocenium couple) was used, and this compartment was separated from the rest of the cell with a Vycor frit. Radical anion solutions were prepared at controlled potential according to the reduction potential of each compound. After 1.0 - 1.1 F per mole of NDI was passed, the anolyte was taken with a syringe and the catholyte (radical anion solution) was transferred to a Schlenk flask that has been connected to the H-cell prior to electrolysis. The obtained RA solution was transferred to UV-Vis cuvettes in a glove box under Argon atmosphere for stationary and transient absorption spectroscopy. Cuvettes were closed with teflon caps using teflon paste to avoid contamination with O_2. Solution of radical anions prepared in this way proved to be stable for at least for 6 h. This feature of radical anion solutions (see next section) are in good agreement with reported data isolated NDI radical anions, this radicals have been isolated and their structure unambiguously determined by x-ray, UV-Vis, and EPR experiments.[6–8]

4.2. Stationary spectroscopy

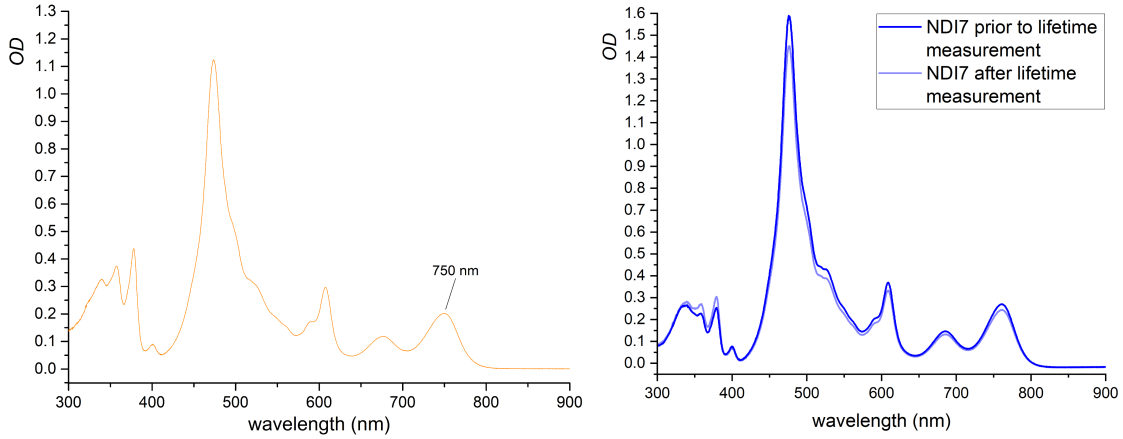

Figure S4. UV-Vis spectra of $NDI2^{\cdot-}$ (left) and of $NDI7^{\cdot-}$ (right) in 0.1 M Bu_4NBF_4 ACN (2 mm cuvette) ([NDI]° ~ 0.25 mM)([NDI7]° ~ 0.43 mM).

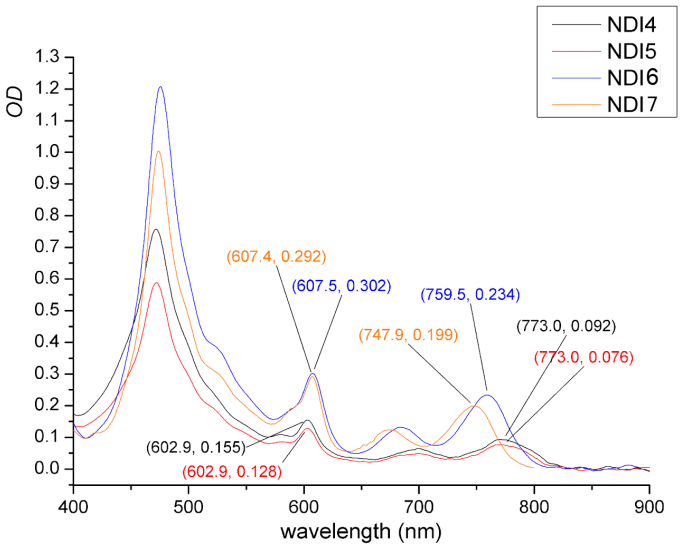

Figure S5. Selected RA UV-Vis spectra from spectroelectrochemical experiments (1 mm cuvette). NDI4, NDI5, NDI6 and NDI7 in 0.1 M Bu_4NBF_4 ACN ([NDI]° ~ 0.5 mM).

4.3. Transient absorption spectroscopy

For femtosecond transient absorption (fsTA) spectroscopy, a setup pumped by a regenerative Ti:sapphire amplifier system (CPS-2001, CLARK MXR) providing ultrashort laser pulses with a repetition rate of 1 kHz, a wavelength of 775 nm and a pulse duration of about 150 fs was used. Ultrashort excitation pulses centered at 680 nm were generated with a noncollinear optical parametric amplifier (NOPA). Their dispersion was minimized by a compressor based on fused-silica prisms resulting in a pulse duration of around 40 fs. The energy of the resulting excitation pulses was around 300 nJ. Absorption changes were probed over the visible spectral range with a white-light continuum generated in a rotating CaF_2-plate. The polarizations of the pump and probe pulses were set to the magic angle (~54.7°) relative to each other. Both pulses were focused onto the sample overlapping spatially there. After passing through the sample, the probe was spectrally dispersed and the fsTA changes were recorded by a photodiode array detector with 512 pixels. The chirp of the probe signal was corrected numerically. The sample solutions were measured in a quartz cuvette with a thickness of 1 or 2 mm (preparation see section 3.1). The obtained data was analyzed using a global fit (global lifetime analysis).

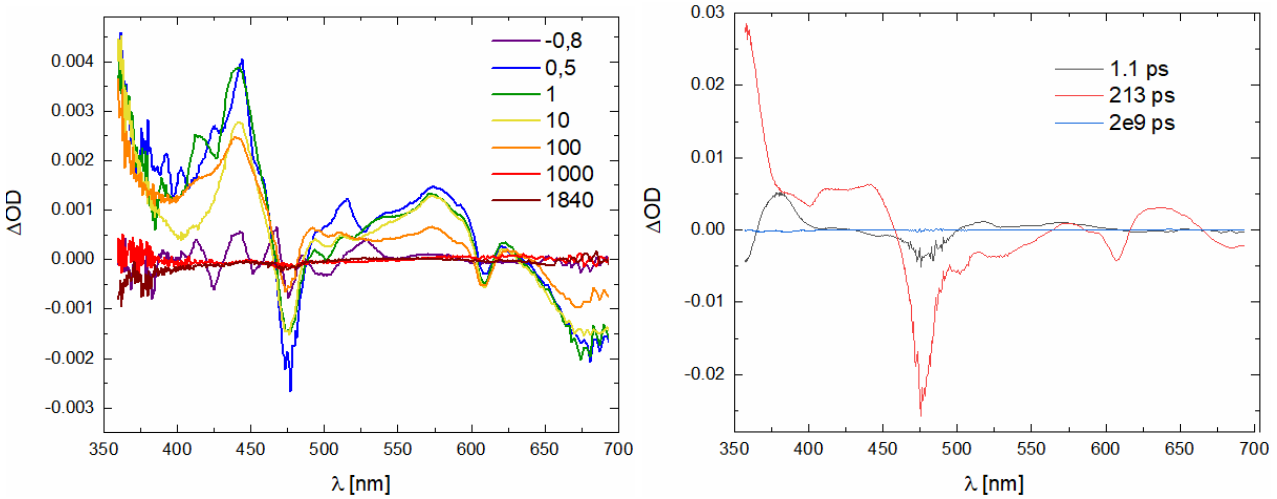

Figure S6. Transient absorption spectra measured for various time delays (given in ps) after 675 nm excitation of $NDI2^{\cdot-}$ in 0.1 M Bu_4NBF_4 ACN ($[NDI]^o \sim 0.4$ mM).

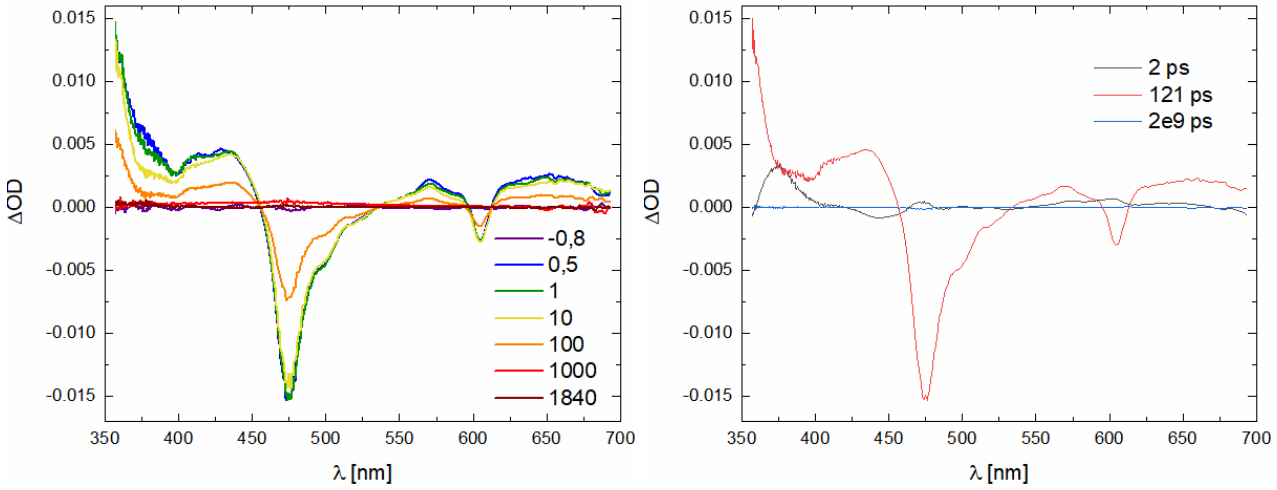

Figure S7. Transient absorption spectra measured for various time delays (given in ps) after 675 nm excitation of $NDI4^{\cdot-}$ in 0.1 M Bu_4NBF_4 ACN ($[NDI]^o \sim 0.4$ mM).

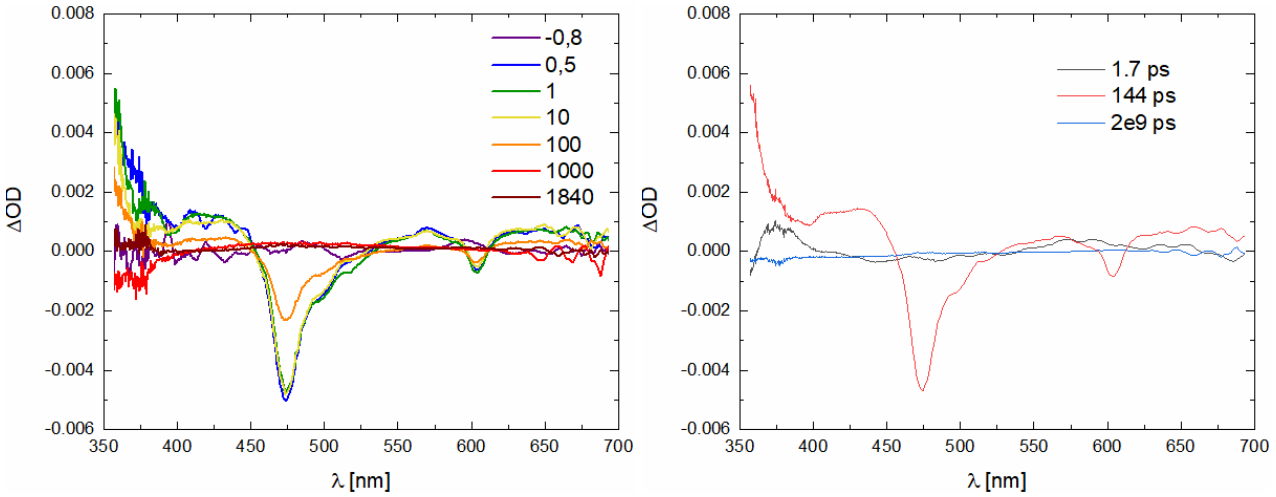

Figure S8. Transient absorption spectra measured for various time delays (given in ps) after 675 nm excitation of $NDI5^{\cdot-}$ in 0.1 M Bu_4NBF_4 ACN ([NDI]º ~ 0.4 mM).

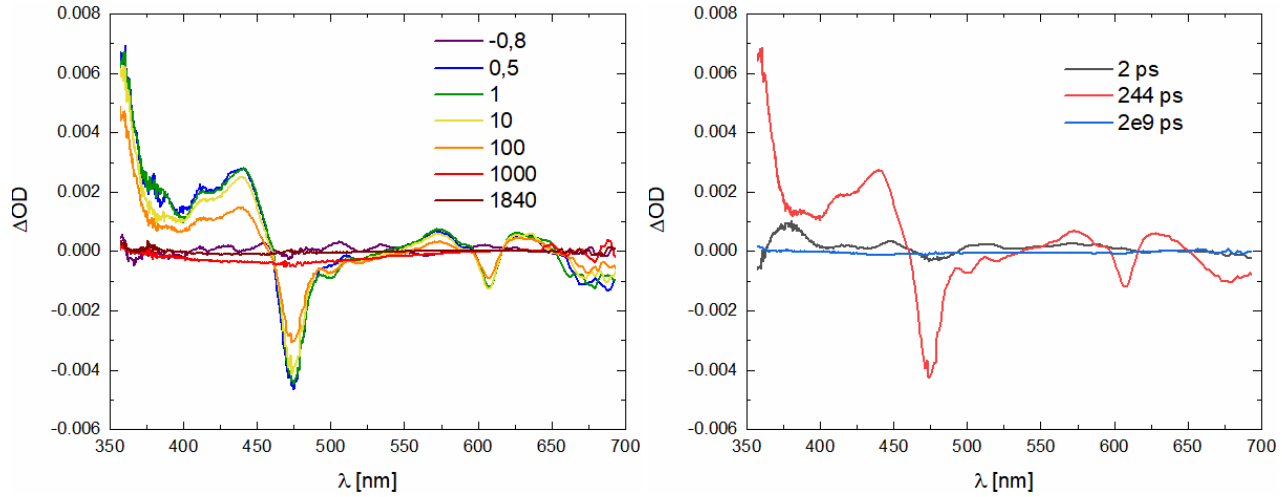

Figure S9. Transient absorption spectra measured various time delays (given in ps) after 675 nm excitation of $NDI6^{\cdot-}$ in 0.1 M Bu_4NBF_4 ACN ([NDI]º ~ 0.4 mM).

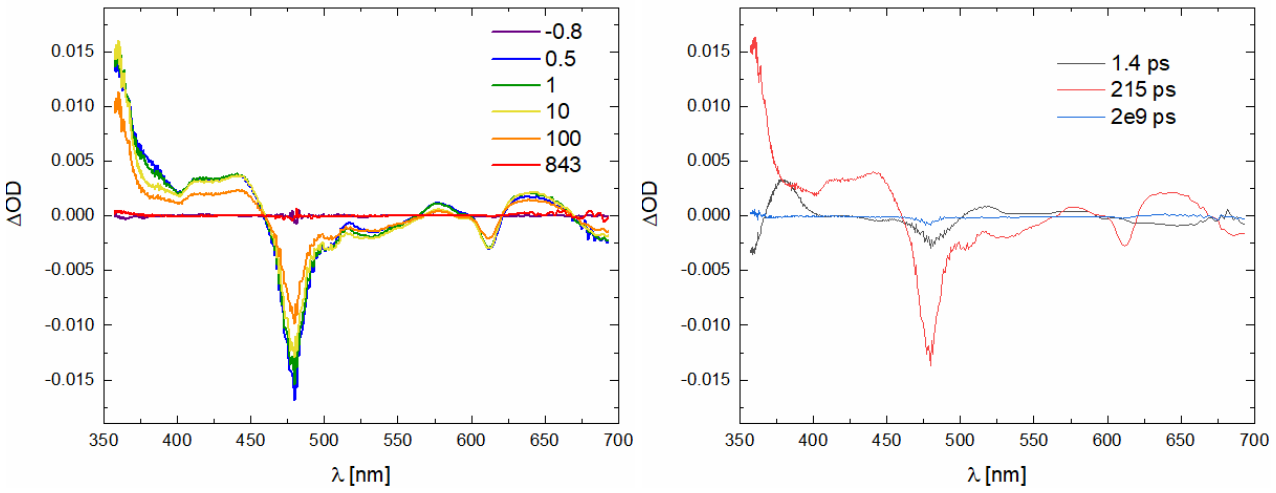

Figure S10. Transient absorption spectra measured for various time delays (given in ps) after 675 nm excitation of $NDI7^{\cdot-}$ in 0.1 M Bu_4NBF_4 ACN ([NDI]º ~ 0.4 mM).

We observe two relevant time constants in all cases. Additionally, we have a very weak long component with infinity lifetime (2e9 ps) to model residual signal like stray light. Nevertheless, the amplitude is so weak that this component is

negligible. The short lifetime $\boldsymbol{\tau_1}$ is in all cases of the order of 2 ps and indicates internal vibrational redistribution (IVR) a very common mechanism when excitation is performed to an vibrational excited state. The present excitation is 680 nm which results in a vibrationally excited state. We associate the lifetime $\boldsymbol{\tau_2}$ to the decay from the first excited state. The amplitude (always red in the amplitude spectra) is in all cases of similar shape with dominant bleach signals (neg. signals) and characteristic red shifted excited state absorptions (positive signals).

Table S2. Transient absorption results.

Compound	τ_1 **[ps]**	τ_2 **[ps]**
NDI2	1.1	213
NDI4	2.0	121
NDI5	1.7	144
NDI6	2	244
NDI7	1.4	215

5. Quantum-chemical calculations

5.1. Computational methods

All calculations were performed with the Gaussian 16 Rev. C.01 suite of programs and MOMAP – MOlecular MAterial Property Prediction Package trial version 2021B. Gaussian calculations were performed in the computational resources from CCAD-Universidad Nacional de Córdoba (https://ccad.unc.edu.ar/) using 1 node of Serafin (2 AMD EPYC 7532 de 200W with 32 cores Zen2 and 128 GiB de RAM DDR4-3200) and 1 node of Eulogia (64 cores KNL Xeon Phi 7210/7250 + 16 GiB MCDRAM and 96 GiB RAM DDR4-2400) servers. Geometry optimizations for all D_0 and D_1 structures were performed employing DFT and LR-TDDFT, respectively, using the UCAM-B3LYP functional in combination with the 6-31+G(d) basis set. The obtained stationary points were characterized by Hessian diagonalization and harmonic frequency analyses to obtain the zero-point and thermal corrections for the energies, enthalpies, and free energies. Solvation effects were simulated using the IEFPCM model with the dielectric constants of *N*,*N*-dimethylformamide and acetonitrile. The excited-state decay rates were calculated using the TVCF formalism (see below) as implemented in the MOMAP-2021B package. The TVCF applies the multidimensional harmonic oscillator approximation, where displacements, distortions and Duschinsky rotation effect (DRE) can be taken into account. For this purpose, adiabatic energies (E_{ad}), transition dipole moments and nonadiabatic coupling matrix elements (NACMEs) were calculated at the UCAM-B3LYP/6-31+G(d) level (Figure S11 and Figure S12). In this work, all rate calculations included DRE. Additionally, calculations using the range-separated ωB97XD (section 6) have been performed for comparative purposes. DFT- optimized coordinates and all output data from calculations are available in the Zenodo repository (https://doi.org/10.5281/zenodo.8092376)

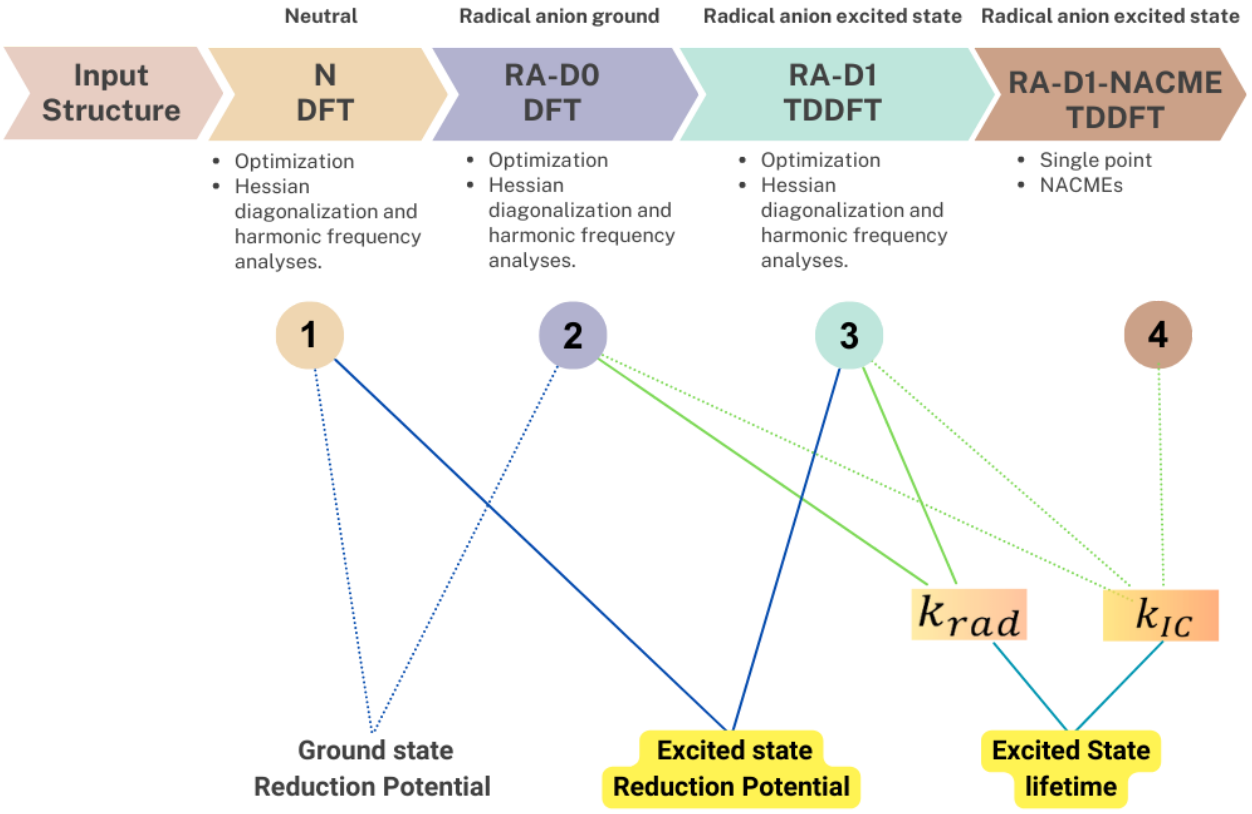

Figure S11. General methodology to obtain excited state lifetimes and potentials.

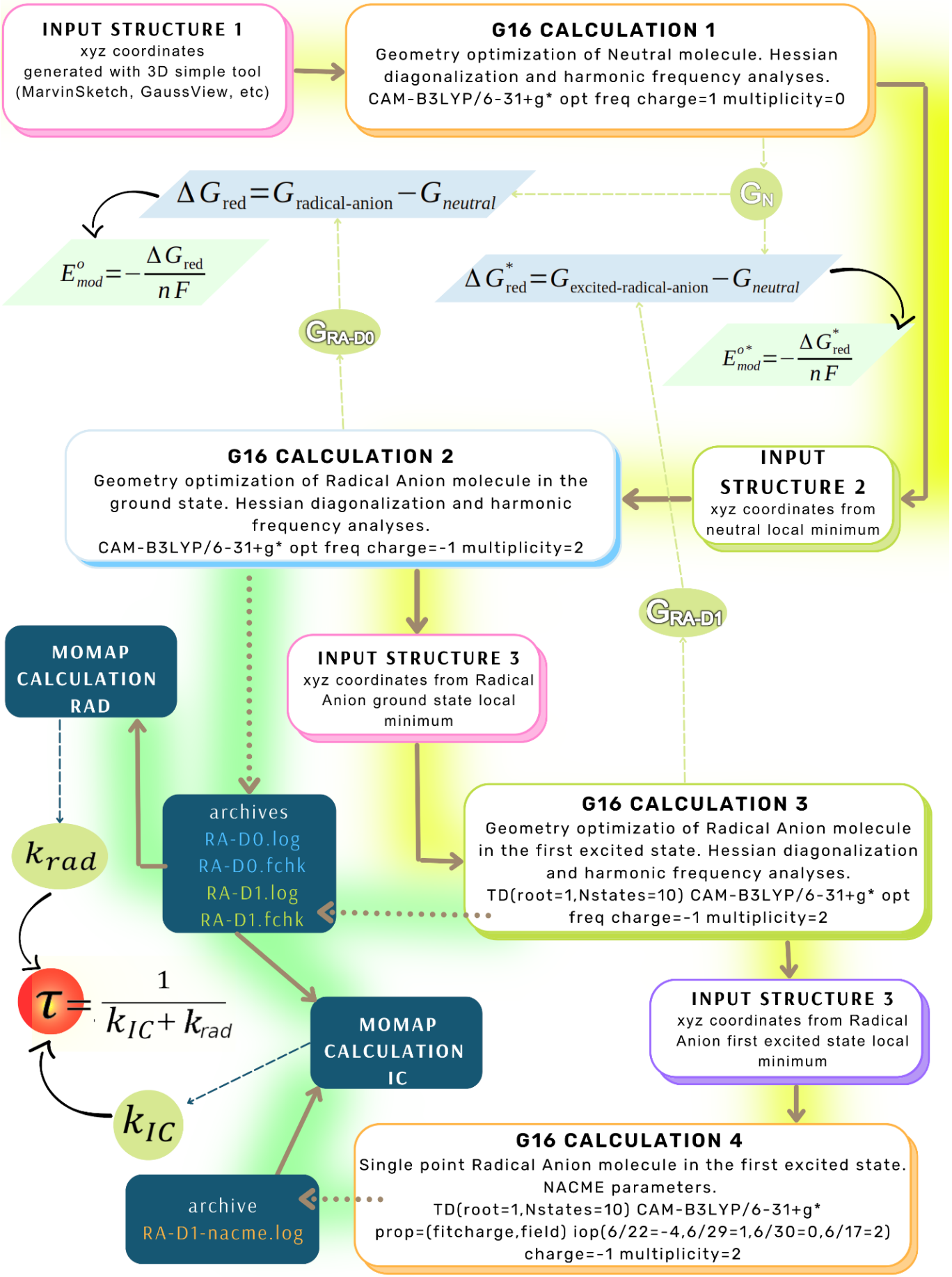

Figure S12. Flow chart for calculation

5.1.1. Computation of excited-state decay rates

In the weak coupling limit, the IC rates (k_{IC}) can be modeled using a combination of Fermi's golden rule and first-order perturbation theory. For this purpose, the Condon approximation was applied and the nonadiabatic coupling (NAC) operator was utilized to account for the interaction between the D_0 and D_1 states. The electronic NAC was evaluated with the *Gaussian 16* code, on the basis of ground and excited-state frequency calculations (Figure S11). The IC rate is given by

$$k_{\mathrm{IC}} = \sum_{r,p} \frac{1}{\hbar} R_{rp} \int_{-\infty}^{\infty} \mathrm{d}t e^{-i\Delta E_{if} t} Z_{iv}^{-1} \rho_{\mathrm{IC},rp}(t, T),$$

where R_{rp} is the nonadiabatic coupling matrix coming from the electronic part of the Condon approximation and the $\rho_{IC,rp}$ part accounts for both the Franck–Condon factors and the nuclear part of the nonadiabatic coupling matrix. This last term is derived from the Thermal Vibration Correlation Function (TVCF) treatment implemented in the *MOMAP* package. More detailed information about the formulations and implementation of the TVCF formalism can be found in ref. 28 and 36 of the main text.

5.2. Optical properties of radical anions

Predicted UV-Vis absorption of radical anions were taken from the computed Excitation Energies of an TD-DFT level energy calculation for the first excited state (root=1) at the geometry of the DFT ground state.

Table S3. Spectroscopic data of naphthalene diimide radical anions.

Entry	Compound	Ref.	Experimental Vertical Absorption energy		Modeled Vertical Absorption energy $D_0 \rightarrow D_1$ (see section 6)	
			λ_{max}^{RA} (nm)[a]	$E_v^{\exp}$ (eV)[b]	E_v^{calc} (eV)	$E_v^{calc} - E_v^{\exp}$
1	NDI1	10.1021/jp000706f	777	1.60	1.88	0.28
2	NDI2 (DMF)	10.1021/jp000706f	755	1.64	1.95	0.31
3	NDI3	10.1021/acs.jpcb.9b06303	749	1.66	1.88	0.22
4	NDI2 (ACN)	this work	755	1.64	1.95	0.31
5	NDI4	this work	773	1.60	1.95	0.35
6	NDI5	this work	773	1.60	1.89	0.29
7	NDI6	this work	760	1.63	1.89	0.26
8	NDI7	this work	750	1.65	1.95	0.30
9	FDI1	10.1021/jp000706f	718	1.73	1.63	-0.10
10	FDI2	10.1021/jp000706f	715	1.73	1.64	-0.09
11	NMI1	10.1021/jacs.1c06844	800	1.55	1.72	0.17
12	DCA	10.1039/d1cp04014f	709	1.75	1.93	0.18
13	TrCA	10.1039/d1cp04014f	715	1.74	1.91	0.17
14	TCA	10.1039/d1cp04014f	715	1.74	1.90	0.16
15	PDI1	10.1021/jp000706f	955	1.30	1.49	0.19
16	PDI2	10.1021/jacs.9b13027	955	1.30	1.49	0.19
17	PMI	10.1021/jp000706f	818	1.52	1.83	0.31

[a] Local maximum of UV-Vis radical anion spectra at the lowest wavelength. [b] Experimental vertical excitation taken

from the local maximum.

As shown in Table S2, the excitation energies are slightly overestimated by 0.16-0.31 eV, a typical behavior of the functionals used.[34] The $D_0 \rightarrow D_1$ excitation, which corresponds to the absorption band between 748 and 777 nm (Figure S4-5), can mainly be characterized as a single electron transition from the SOMO to the LUMO (Figure S12). In all cases, the analyses of molecular orbitals and transition densities (Figures S15-S16) reveal that the D_1 state exhibits a $\pi\pi^*$ of local character, centered on the NDI core.

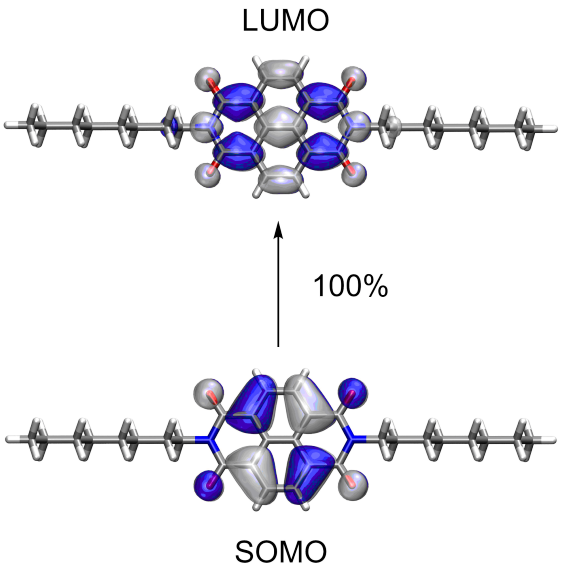

Figure S13. Single electron transition from the SOMO to the LUMO of NDI2.

5.3. Studies on the electrochemical properties of RAs

5.3.1. Calculation of excited state redox potential

Data for the ground state reduction potential couple $M/M^{\cdot-}$ (E^o_{exp}) were taken from cyclic voltammetry measurements (section Electrochemical properties of NDI).

$$e^- + M \longrightarrow M^{-\cdot} \qquad E^o_{exp}$$

Data for the excited state reduction potential couple $M/M^{\cdot-}$* (E^{o*}_{exp}) were calculated according to the equation S1

$$e^- + M \longrightarrow M^{-\cdot *} \qquad E^{o*}_{exp}$$

$$E^{o*}_{exp} = E^o_{exp} - E^{0\text{-}0} \quad (\text{eq S1})$$

where $E^{0\text{-}0}$ corresponds to the difference between the first excited state and the ground state. $E^{0\text{-}0}$ was approximated by the energy of the lowest-wavelength local maximum in the UV-Vis spectra of radical anions (Table S3). These values correspond to the vertical excitation energy and the values of $E^{0\text{-}0}$ are overestimated. We decided to take this approach due to the lack of fluorescence data which would allow a better estimation of $E^{0\text{-}0}$ based on the intercept of UV-Vis and fluorescence spectra. The use of the onset value was avoided due to limited access to all numerical experimental UV-Vis spectra of the compounds not synthesized in this work, which and make a "manual" determination of the onset challenging and more prone to errors (https://www.sciencedirect.com/science/article/pii/S0022407321000376) than the maximum. .

5.3.2. Computationally predicted electrochemical properties

Data for the modeled ground state reduction potential couple $M/M^{\cdot-}$ (E^{o}_{mod}) and the excited state reduction potential couple $M/M^{\cdot-}$* (E^{o}_{mod}*) were obtained through the change in the Gibbs free energy of the involved species:

$$E^{o}_{mod} = -\frac{\Delta G_{red}}{nF} \qquad \Delta G_{red} = G_{radical\text{-}anion} - G_{neutral}$$

$$E^{o*}_{mod} = -\frac{\Delta G^{*}_{red}}{nF} \qquad \Delta G^{*}_{red} = G_{excited\text{-}radical\text{-}anion} - G_{neutral}$$

Modeled potentials were related to NHE electrode in ACN by subtraction of 4.6 V according to Ref. 37.

$$E^{o}_{mod}(vs\ NHE) = E^{o}_{mod} - 4.6\,V$$

Table S4. Electrochemical properties of RAs.

Entry	Name	E^{o}_{exp} [V]	Ref.	E^{o}_{exp} [V] (*vs.* NHE)	E^{o}_{mod} [V] (*vs.* NHE)	E^{o*}_{exp} [V] (*vs.* NHE)	E^{o*}_{mod} [V] (*vs.* NHE)
1	NDI1	-0.48[a]	10.1021/jp000706f	-0.24	-0.70	-1.83	-2.37
2	NDI2	-0.48[a]	10.1021/jp000706f	-0.24	-0.70	-1.88	-2.40
3	NDI2	-0.92[b]	this work	-0.37	-0.73	-2.01	-2.41
4	NDI4	-0.87[b]	this work	-0.32	-0.98	-1.92	-2.55
5	NDI5	-0.88[b]	this work	-0.33	-0.73	-1.93	-2.30
6	NDI6	-0.92[b]	this work	-0.37	-0.48	-2.03	-2.02
7	NDI7	-0.94[b]	this work	-0.39	-0.73	-2.02	-2.41
8	FDI1	-0.71[a]	10.1021/jp000706f	-0.47	-0.94	-2.20	-2.22
9	FDI2	-0.71[a]	10.1021/jp000706f	-0.47	-0.95	-2.19	-2.32
10	NMI1	-1.25[c]	10.1002/anie.202105895	-1.45	-1.57	-3.00	-3.09
11	DCA	-0.67[b]	10.1021/jo071157d	-0.67	-0.98	-2.42	-2.55
12	TrCA	-0.43[b]	10.1021/jo071157d	-0.43	-0.73	-2.17	-2.30
13	TCA	-0.20[b]	10.1021/jo071157d	-0.20	-0.48	-1.94	-2.02
14	PDI1	-0.43[a]	10.1021/jp000706f	-0.19	-0.68	-1.48	-1.88
15	PDI2	-0.88[d]	10.1126/science.1258232	-0.23	-0.66	-1.53	-1.86
16	PMI	-0.96[a]	10.1021/jp000706f	-0.72	-1.15	-2.24	-2.74

[a] *vs.* SCE in DMF. [b] *vs.* $Ag/AgNO_3$ (0.01 M) in ACN. [c] *vs.* Ag/AgCl in propylene carbonate. [d] *vs.* Fc/Fc^{+} in ACN.

5.4. Photophysical properties of excited radical anions

The decay rates and lifetimes were calculated using the TVCF formalism, as implemented in the *MOMAP-2021B* program package.

Table S5. Summary of photophysical properties.

Entry	Name	Ref.	τ_{exp}[a] (ps)	τ_{mod}[b] (ps)	k_{IC}[c] (s^{-1})	k_{rad}[d] (s^{-1})	Adiabatic Energy (hartree)	Total λ	EDMA[e]	EDME[f]
1	NDI1	10.1021/jp000706f	141[g]	137	7.3E+09	1.1E+07	6.20E-02	1563	4.18	4.62
2	NDI2 (DMF)	10.1021/jp000706f	260[g]	197	5.1E+09	1.2E+07	6.48E-02	1549	4.18	4.62
3	NDI3	10.1021/acs.jpcb.9b06303	103[h]	73[g]	1.4E+10	9.9E+06	6.22E-02	1537	4.25	4.69
4	NDI2 (ACN)	this work	213[h]	200	5.0E+09	1.2E+07	6.48E-02	1549	4.18	4.61
5	NDI4	this work	121[h]	46	2.2E+10	9.6E+06	6.24E-02	1544	4.32	4.76
6	NDI5	this work	144[h]	82	1.2E+10	1.0E+07	6.25E-02	1545	4.32	4.76
7	NDI6	this work	244[h]	196	5.1E+09	1.2E+07	6.48E-02	1551	4.18	4.62
8	NDI7	this work	215[h]	171	5.9E+09	1.1E+07	6.37E-02	1549	4.15	4.58
9	FDI1	10.1021/jp000706f	6[g]	0.28	3.6E+12	3.3E+06	4.99E-02	2269	0.00	4.66
10	FDI2	10.1021/jp000706f	9[g]	0.75	1.3E+12	6.0E+06	5.17E-02	2173	8.01	5.55
11	NMI1	10.1021/jacs.1c06844	24[i]	9.1[g]	1.1E+11	9.2E+06	5.56E-02	1698	4.67	5.22
12	DCA	10.1039/d1cp04014f	3[h]	10.7	9.4E+10	1.1E+07	6.10E-02	2146	4.90	5.82
13	TrCA	10.1039/d1cp04014f	5[h]	9.4	1.1E+11	9.6E+06	6.13E-02	2019	4.14	5.38
14	TCA	10.1039/d1cp04014f	3[h]	19	5.3E+10	9.7E+06	6.03E-02	2001	4.63	5.38
15	PDI1	10.1021/jp000706f	141[g]	0.74	1.4E+12	2.2E+07	4.48E-02	2027	10.70	13.02
16	PDI2	10.1021/jacs.9b13027	160[g]	0.79	1.3E+12	2.2E+07	4.47E-02	2023	10.65	12.98
17	PMI	10.1021/jp000706f	533[g]	21	4.8E+10	9.2E+06	6.02E-02	1597	4.34	4.78

[a] Experimental radical anion excited state lifetime. [b] Modeled radical anion excited state lifetime. [c] Modeled internal conversion rate constant $D_1 \rightarrow D_0$. [d] Modeled radiative rate constant $D_1 \rightarrow D_0$. [e] Modeled electronic dipole moment of absorption. [f] Modeled electronic dipole moment of emission. [g] DMF. [h] ACN. [i] Propylene carbonate.

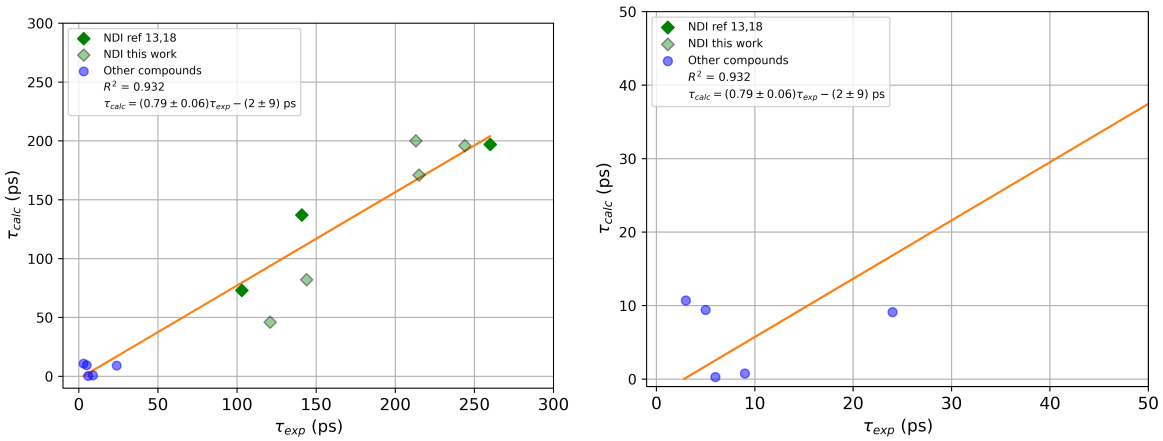

Figure S14. Correlation between experimental (τ_{exp}) and calculated (τ_{calc}) lifetimes (entries 1-14 Table S5)

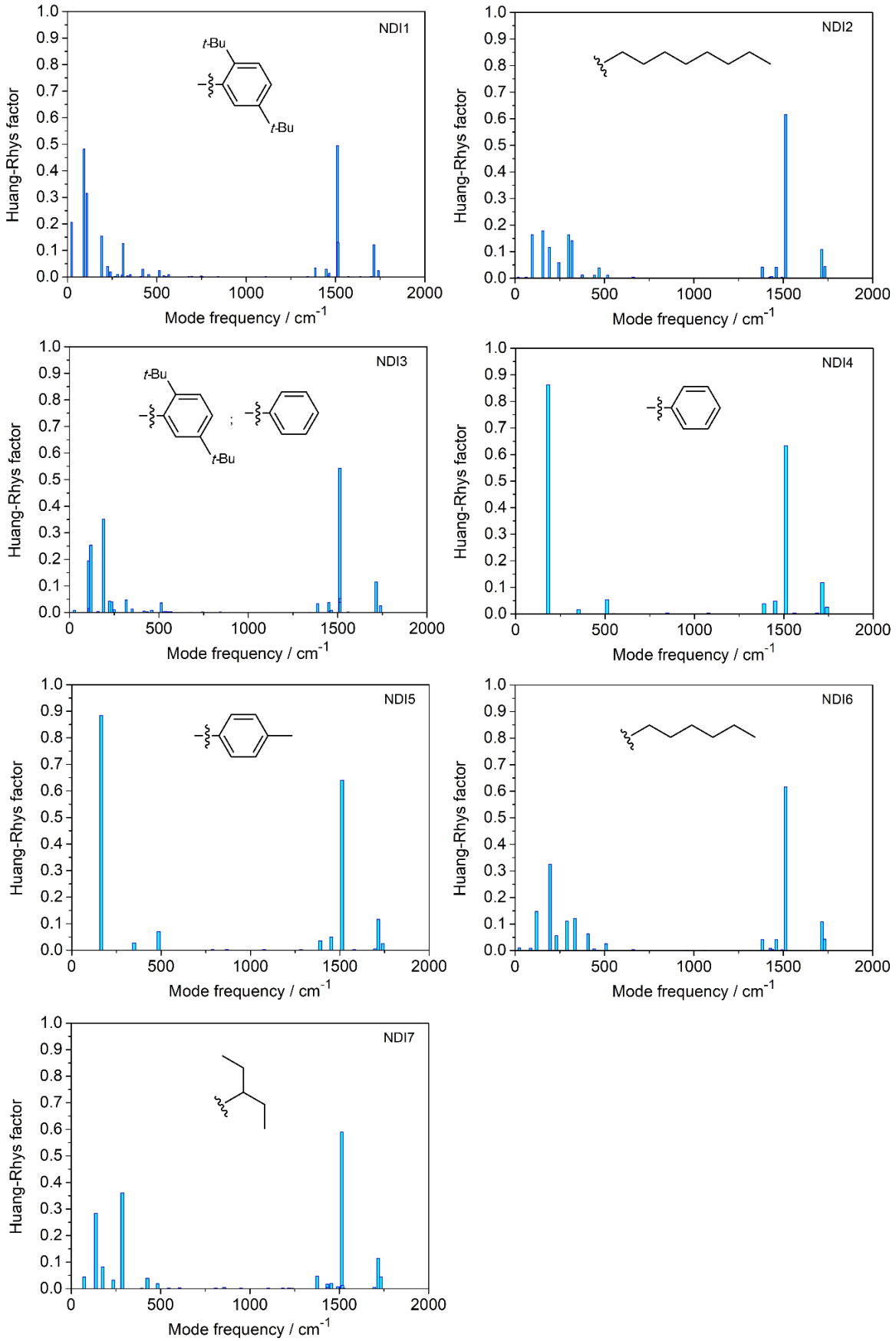

Figure S15. Huang-Rhys factors for the relevant vibrational modes computed at the D_1 equilibrium geometries of NDIs 1-7. Inset: groups attached at the *imide* position of NDIs except for NDI3, all the NDIs are symmetrically substituted. (See Figure S1-2).

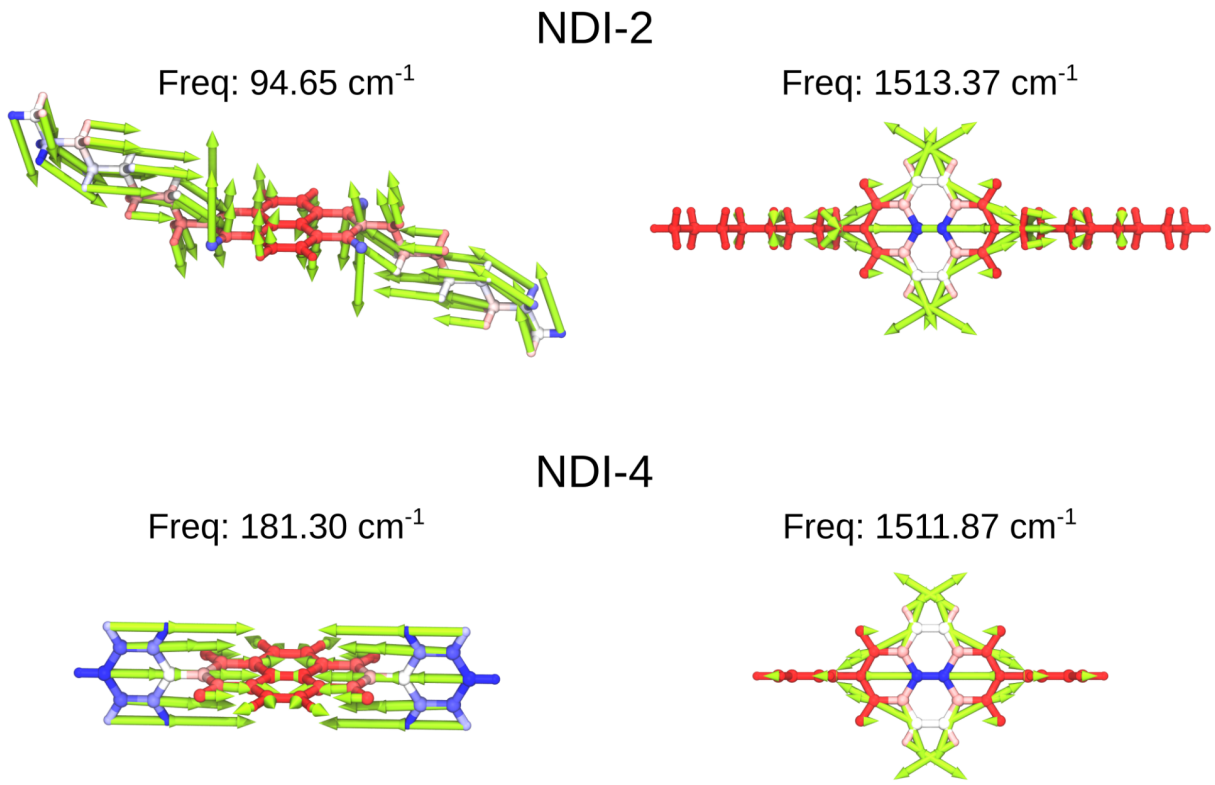

Figure S16. Normal mode relevant for the deactivation of the D_1 state.

Huang-Rhys (HR) factor describes the extent of geometry relaxation between two electronic states and thus it is ultimately related to the strength of vibronic coupling. This factor can be used to estimate the energy dissipation during the vibrational relaxation process in an excited state (known as the internal reorganization energy, λ), which particularly affects the nonradiative decay rate. For the NDI series, the HR distribution profiles in the D_1 state show a large contribution from the high-frequency region (around 1500 cm^{-1}, Figure S13), together with smaller contributions from the low-frequency domain (below 500 cm^{-1}). Interestingly, the stretching mode at 1500 cm^{-1} for NDI2 (with aliphatic groups) and for NDI4 (with aromatic groups) is essentially identical in both cases, involving the deformation of the naphthalene core (Figure S14). More importantly, in the case of NDI4, a stretching mode centered on the aromatic groups (Figure S14) presents the higher HR value (Figure S13), implying that the aromatic groups could play a significant role in the vibrational nonradiative IC process. Conversely, for NDIs RAs having aliphatic groups (such as NDI2, Figure S14), the role of the side chains in the vibrational coupling seems to be considerably lower, which is related to their slightly longer excited-state lifetimes.

Table S6. Summary of photophysical properties for compounds of Figure 3b.[a]

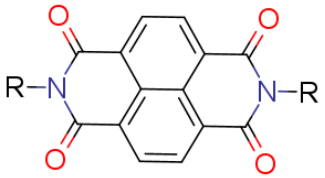

Entry	Name	R	τ_{mod}[b] (ps)	k_{IC}[c] (s^{-1})	k_{rad}[d] (s^{-1})	Adiabatic Energy (hartree)	Total λ	EDMA[e]	EDME[f]
1	NDI-0	H	15	6.55E+10	1.04E+07	6.34E-02	1548	4.470936	4.922965
2	NDI-11	Me	76	1.31E+10	1.11E+07	6.53E-02	1552	4.252014	4.693826
3	NDI-12	Et	174	5.75E+09	1.16E+07	6.50E-02	1551	4.227482	4.664556
4	NDI-15	n-propil	178	5.60E+09	1.16E+07	6.49E-02	1551	4.210485	4.646239
5	NDI-16	n-butil	177	5.63E+09	1.15E+07	6.49E-02	1551	4.197885	4.634335
6	NDI-17	n-pentil	189	5.27E+09	1.16E+07	6.48E-02	1552	4.191185	4.627709
7	NDI-13	i-propil	125	8.00E+09	1.10E+07	6.40E-02	1552	4.201577	4.650964
8	NDI-14	t-butil	11	8.70E+10	7.21E+06	5.75E-02	1763	4.170015	4.574495

[a] Values modeled in DMF. [b] Modeled radical anion excited state lifetime. [c] Modeled internal conversion rate constant $D_1 \rightarrow D_0$. [d] Modeled radiative rate constant $D_1 \rightarrow D_0$. [e]

Figure S17. Optimized structure of NDI-14 radical anion in the excited state D_1.

5.5. Modeling of excited state quartet of NDI2 and comparison with D_1

Geometry optimization for Q_1 state structure of $NDI2^{\cdot -}$ was performed employing DFT, using the UCAM-B3LYP functional in combination with the 6-31+G(d) basis set. A comparison with the D_1 state in terms of Gibbs free energies is shown in Table S7.

Table S7. Comparison of Q_1 and D_1 of $NDI2^{\cdot -}$.

Entry	State	G (kcal mol^{-1})	$\Delta G(Q_1\text{-}D_1)$(kcal mol^{-1})
1	D_1	-988560.4	-
2	Q_1	-988529.0	31.4

5.6. PDI and PMI cases

Data for perylene core compounds could not be reproduced within the limits of the present method. This failure seems to be associated with an overestimated relaxation energy rather than a large error in the adiabatic energy. This is supported by the similar agreement of optical (Table S3) and energetic parameters (Table S4) compared to the rest of the compounds. This could be further illustrated by the dependency of τ_{mod} with respect of adiabatic energy for PDI2 (Table S8) in which the rest of the parameter are kept constant. This analysis predicts an adiabatic energy > 0.071 Hartree to match the experimental value. This value is larger than the one obtained for the NDI family (< 0.0648) which is unlikely in view of the smaller size of the conjugated diimide system. The exact reason for overestimation is unclear but seems to be general for the DFT method (see section 6).

Table S8. Dependency of τ_{mod} with respect of adiabatic energy for PDI2.

Entry	Adiabatic Energy (hartree)	τ_{mod} (ps)	% deviation from calculated value
1	4.47E-02	0.79	100%
2	4.92E-02	1.56	110%
3	6.26E-02	17.5	140%
4	7.16E-02	105	160%
5	7.25E-02	126	162%
6	7.61E-02	260	170%
7	8.05E-02	260	180%

6. Extra Calculations

6.1. Calculations at the ωB97XD/6-31+G(d) level

Table S9. Summary of modeled photophysical properties with ωB97XD/6-31+G(d).

Entry	Name	τ_{mod}[b] (ps)	k_{IC}[c] (s^{-1})	k_{rad}[d] (s^{-1})	Adiabatic Energy (hartree)	Total λ	EDMA[e]	EDME[f]
1	NDI1[g]	149	6.70E+09	1.07E+07	6.25E-02	1566	4.17	4.62
2	NDI2[g]	153	6.53E+09	1.14E+07	6.49E-02	1581	4.18	4.62
3	NDI3[h]	92	1.09E+10	1.05E+07	6.26E-02	1567	4.24	4.69
4	NDI2[h]	153	6.54E+09	1.13E+07	6.49E-02	1581	4.18	4.62
5	NDI4[h]	75	1.33E+10	1.02E+07	6.26E-02	1550	4.32	4.77
6	NDI5[h]	2.5	4.01E+11	9.10E+06	6.27E-02	1570	4.32	4.77
7	NDI6[h]	202	4.94E+09	1.19E+07	6.49E-02	1585	4.18	4.62
8	NDI7[h]	58	1.72E+10	1.05E+07	6.40E-02	1568	4.14	4.58
9	FDI1[g]	0.34	2.94E+12	3.64E+06	4.94E-02	2264	1.70	4.79
10	FDI2[g]	0.65	1.55E+12	5.54E+06	5.08E-02	2213	8.09	5.49
11	NMI1[i]	0.87	1.15E+12	7.65E+06	5.57E-02	1704	4.68	5.23
12	DCA[h]	2.8	3.63E+11	1.07E+07	6.22E-02	2168	4.87	5.80
13	TrCA[h]	2.3	4.31E+11	9.60E+06	6.24E-02	2050	4.13	5.38
14	TCA[h]	10	9.74E+10	9.65E+06	6.16E-02	2036	4.58	5.36
15	PDI1[g]	0.25	4.06E+12	1.68E+07	4.58E-02	2081	10.48	13.22
16	PMI[g]	0.89	1.12E+12	7.03E+06	6.03E-02	1673	4.35	4.80

[a] [b] Modeled radical anion excited state lifetime. [c] Modeled internal conversion rate constant $D_1 \rightarrow D_0$. [d] Modeled radiative rate constant $D_1 \rightarrow D_0$. [e] Modeled electronic dipole moment of absorption. [f] Modeled electronic dipole moment of emission. [g] DMF. [h] ACN. [i] Propylene carbonate.

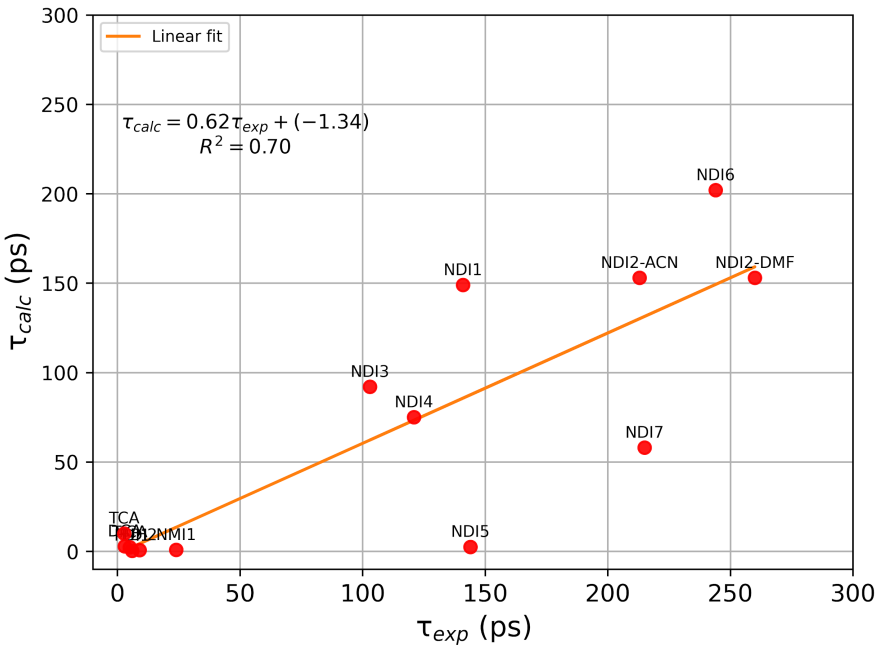

Figure S18. Correlation between experimental (τ_{exp}) and calculated (τ_{calc}) lifetimes (entries 1-14 Table S9).

7. References

1 S.-L. Suraru and F. Würthner, *Angew. Chem. Int. Ed.*, 2014, **53**, 7428–7448.
2 S. Guha, F. S. Goodson, L. J. Corson and S. Saha, *J. Am. Chem. Soc.*, 2012, **134**, 13679–13691.
3 D. Shukla, S. F. Nelson, D. C. Freeman, M. Rajeswaran, W. G. Ahearn, D. M. Meyer and J. T. Carey, *Chem. Mater.*, 2008, **20**, 7486–7491.
4 S. Guha, F. S. Goodson, S. Roy, L. J. Corson, C. A. Gravenmier and S. Saha, *J. Am. Chem. Soc.*, 2011, **133**, 15256–15259.
5 V. V. Pavlishchuk and A. W. Addison, *Inorganica Chimica Acta*, 2000, **298**, 97–102.
6 Y. Kumar, S. Kumar, D. Bansal and P. Mukhopadhyay, *Org. Lett.*, 2019, **21**, 2185–2188.
7 S. Kumar and P. Mukhopadhyay, *Green Chem.*, 2018, **20**, 4620–4628.
8 Y. Kumar, S. Kumar, K. Mandal and P. Mukhopadhyay, *Angew. Chem. Int. Ed.*, 2018, **57**, 16318–16322.